TOPOGRAPHIC CORRECTION OF LAPAN-A3/LAPAN-IPB MULTISPECTRAL IMAGE: A COMPARISON OF FIVE DIFFERENT ALGORITHMS

ZYLSHAL ZYLSHAL ⃝iD

Remote Sensing Technology and Data Center, Indonesian National Institute of Aeronautics and Space (LAPAN), Jakarta Timur, Indonesia

ABSTRACT: Reflectance variability in mountainous regions caused by steep slopes can decrease the accuracy of landcover mapping. Topographic correction aims to reduce this effect, and various techniques have been proposed to conduct such correction on satellite imagery. This paper presents the initial results of five different topographic correction techniques applied to LAPAN-A3 multispectral images, namely cosine correction, improved cosine correction, Minnaert correction, modified Minnaert correction and two-stage normalization. The widely-available ALOS World 3D 30 meter DEM was employed, with the evaluation made in a mountainous area in South Sulawesi, Indonesia, located in an ancient volcanic region, with slopes ranging from 0 to 60 degrees. The slope aspect was almost equally distributed in all directions. Visual and statistical analysis was conducted before and after the topographic correction to evaluate the results. Standard deviation (SD) and the coefficient variation (CV) were calculated; the results show that the topographic corrections were able to reduce the effect of shadows and relief. Minnaert correction proved to be the best method in terms of visual appearance and spectral variability reduction.

KEY WORDS: LAPAN-A3/LAPAN-IPB, AW3D30, Minnaert, cosine correction, two-stage normalization, coefficient of variation

Corresponding author: Zylshal Zylshal, zylshal@lapan.go.id

Introduction

The latest generation of Indonesian satellite known as LAPAN-A3/LAPAN-IPB was launched in October 2016. This experimental microsatellite carries a multispectral sensor called the Line Imager Space Application (LISA) among several other sensors. The LISA sensor is a push-broom scanner with 15 meter spatial resolution and four bands, ranging from blue visible to near infrared (Zylshal et al. 2018). One of the missions of the satellite is to monitor forests and agricultural land (Judianto and Nasser 2015). Consistent reflectance values of the Earth's surface are important in order to perform forest monitoring using Earth Observation (EO) satellite data (Li et al. 2013). However, in mountainous regions, it can be difficult to obtain such consistent values, especially where there are different facing slopes. Slopes that are directly oriented towards the sun receive more light than those facing away from it, thus making them appear brighter in images (Holben and Justice 1980, Vázquez-Jiménez et al. 2017). This phenomenon has been acknowledged and studied extensively. (Vanonckelen et al. 2013) and (Vanonckelen et al. 2014) provide

a comprehensive list of proposed algorithms to compensate for the topographic effect in EO satellite data.

Out of the vast choice of algorithms, five are most commonly used for topographic correction: cosine correction (Teillet et al. 1982), improved cosine correction (Civco 1989), Minnaert correction (Minnaert 1941), modified Minnaert correction (Riaño et al. 2003), and two-stage normalization (Civco 1989, Law and Nichol 2004). These algorithms are easily accessible on several open source software platforms, including SAGA GIS®, QuantumGIS and GrassGIS.

Although many studies have been conducted on LAPAN-A3 data processing and data applications, only one focuses on topographic correction. The initial assessment by Zylshal (2019) focused on the DEM source for one topographic correction algorithm (Minnaert correction) rather than the algorithm itself. The initial results showed that ALOS World 3D 30 m performed the best on LAPAN-A3. Therefore, this study employs the aforementioned DEM. However, how well other topographic correction algorithms perform on LAPAN-A3 data has not been extensively studied. It is common practice to investigate what is the best topographic correction methods that work with specific satellite data are. Studies on Landsat TM (Justice et al. 1981, Pimple et al. 2017), Landsat-8 OLI (Vincini and Frazzi 2003, Hantson and Chuvieco 2011, Gao et al. 2016, Fan et al. 2018), ALOS AVNIR-2 (Ghasemi et al. 2011), CBERS-2B (Shao et al. 2015), SPOT-5 HRVIR (Soenen et al. 2008), Ikonos (Nichol and Hang 2013), IRS-P6 AWiFS (Mishra et al. 2009), ZY-3 (Gao et al. 2013), Hyperion ALI (Gao et al. 2016), and Quickbird (Wu et al. 2008) have assessed different topographic correction algorithms to find which perform best on their respective data. The studies found that different algorithms worked best with different datasets. The initial results on LAPAN-A3 (Zylshal 2019) were focused on different DEM sources using Minnaert correction (Minnaert 1941), instead of the topographic correction algorithms themselves. Therefore, four out of the five previously mentioned topographic correction algorithms have never been tested on LAPAN-A3 data. LAPAN-A3 studies have focused on various topics, and can generally be divided into three categories:

1. studies focusing on the imaging technology as well as the satellite operational technology (Hasbi and Suhermanto 2013, Hakim et al. 2014, Roza et al. 2014, Judianto and Nasser 2015, Tahir et al. 2016),
2. those focusing on the multispectral image processing (radiometric or spectral characteristics) (Judianto and Nasser 2015, Triharjanto et al. 2016, Hakim and Permala 2017, Hakim et al. 2017, Zylshal et al. 2017, Zylshal 2019),
3. studies focusing on multispectral image applications (Nugroho et al. 2018, Setiawan et al. 2018, Zylshal et al. 2018).

Several topographic correction methods require the satellite imagery to be atmospherically corrected (surface reflectance) (Richter 1997, Riaño et al. 2003, Vanonckelen et al. 2014, Pimple et al. 2017, Vázquez-Jiménez et al. 2017, Phiri et al. 2018). However, the use of top-of-atmosphere (TOA) reflectance is also fairly common (Richter et al. 2009). Designed as an experimental satellite, to date the necessary parameters needed to perform atmospheric correction are not yet available on LAPAN-A3. A comprehensive study of atmospheric correction on LAPAN-A3, while very important, is unfortunately outside the scope of this paper. Considering the importance of topographic correction of satellite imagery, as discussed in the previous paragraph, the digital number (DN) value has been employed in this study (Justice et al. 1981). The output of this study can act as a first step in the right direction, as it evaluates five different topographic correction algorithms.

It is necessary to investigate what algorithm performs best when correcting the topographic effect in LAPAN-A3. This paper aims to compare five common topographic correction algorithms and evaluate which of these performs the best.

Materials and method

Location and Data

The study was conducted in South Sulawesi Province, Indonesia, which is located in the middle of Indonesian archipelago in an ancient and currently inactive volcanic region. The volcanic rock formation is geologically known as Baturappe-Cindakko (Tpbv), as shown in Figure 1. The slope area comprised mostly of agricultural
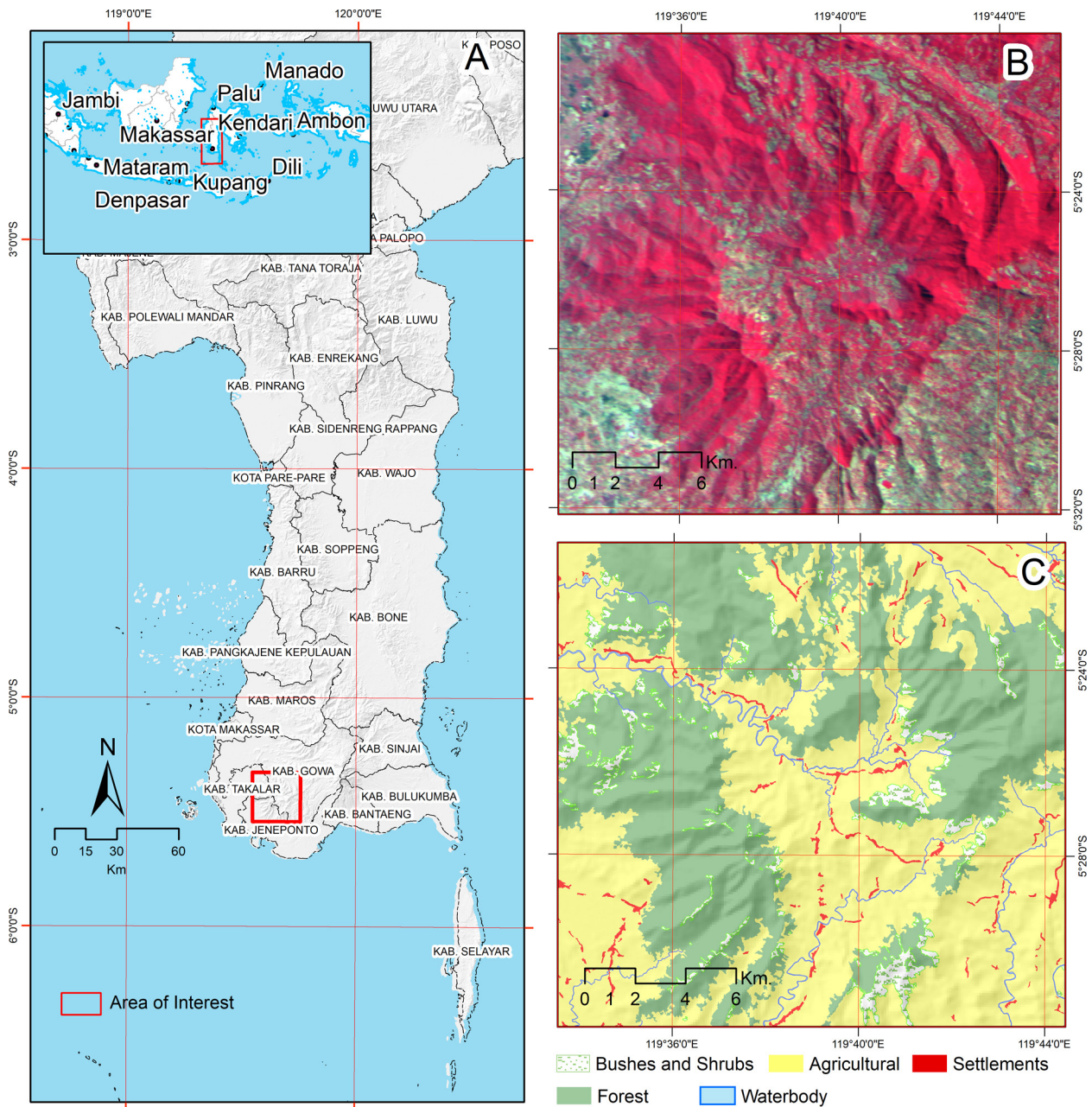
Fig. 1. Study area.
A – Overview of study area on South Sulawesi, Indonesia. B – LAPAN-A3 RGB composite of NIR-R-G, C – Landuse/landcover of the study area taken from visually interpreted SPOT-6 pansharpened iamge (1.5 meter) acquired at September 14th 2019. Red rectangle in left image indicates the area of interest. The right image is the LAPAN-A3 RGB composite of NIR-R-G.

land (53%) and forest (41%). Small portions of the study area are also covered with bushes and shrubs (4%), settlements (1.5%), as well as water-body (0.5%) as shown in Figure 1C. The relief is undulating, with slopes varying from 0 to more than 60 degrees (Fig. 2A, 2B, 2D, 2E). A 23×23 km rectangular subset was chosen as the area of in-terest (AOI). The AOI was specifically selected at mountainous region with different facing slopes

to better understand the effect of topographic correction (Fig. 2C and 2F).

The LAPAN-A3/LAPAN-IPB (LA3) used in this study were acquired on August 28th 2019 at 09.34 AM local time. The solar azimuth was at 69.4437°, with an elevation of 50.75°. LA3 has four spectral bands, ranging from blue to near infra-red. The spatial resolution is 15 meters (Zylshal et al. 2018), and the LA3 imagery came with WGS84
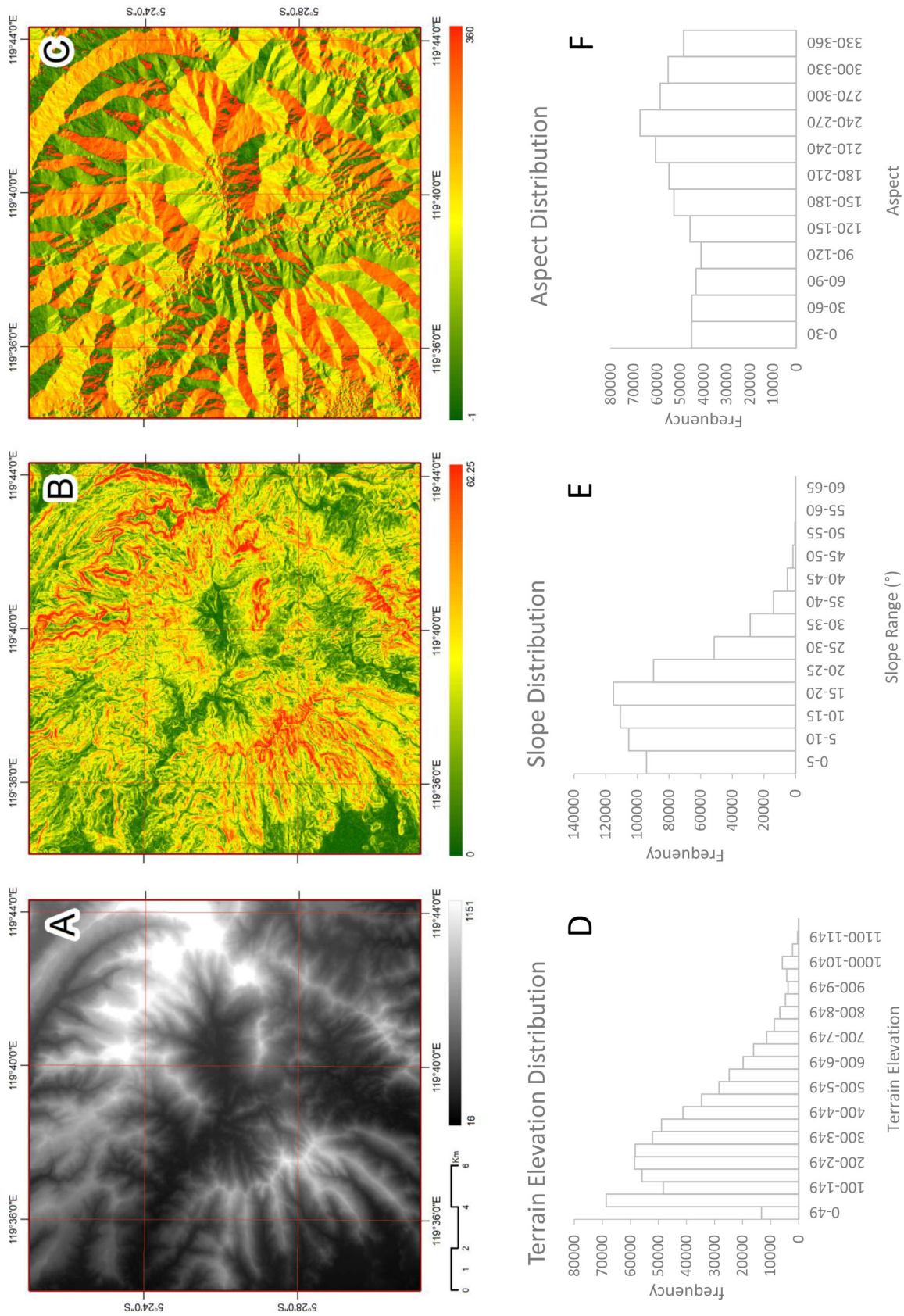
Fig. 2. The terrain elevation and its derivatives used in this study.
A – ALOS World 3D 30 meter, B – Slope map, C – Aspect map, D – Histogram distribution of terrain elevation based on AW3D30, E – Histogram distribution of slopes, F – Histogram distribution of aspects.

projection. After geometric correction, the LA3 data was then transformed into UTM projection (Zone 50 South).

For the chosen correction methods, terrain elevation information is needed in order to simulate the acquisition lighting conditions. Various digital elevation models (DEMs) are available free of charge and cover almost the entire globe; namely, the Shuttle Radar Topographic Mission (SRTM); the ASTER Global Digital Elevation Map (GDEM); and the ALOS Global Digital Surface Model (AW3D30). The latter is currently the newest freely available dataset, being released in March 2017. It utilizes the Advanced Land Observing Satellite (ALOS), specifically the PRISM (Panchromatic Remote-sensing Instrument for Stereo Mapping), to compute the elevation, which delivers with approximately 30 meters of spatial resolution (Japan Aerospace Exploration Agency 1997, Takaku et al. 2016, JAXA 2017, Takaku and Tadono 2017). The DEM was used to compute the slope and aspect of the terrain; a previous study found that AW3D30 performed the best (Zylshal 2019).

Preprocessing

Most previous studies were performed on orthorectified images (Riaño et al. 2003, Gao and Zhang 2009a, Richter et al. 2009, Hantson and Chuvieco 2011, Balthazar et al. 2012, Nichol and Hang 2013, Vanonckelen et al. 2013, 2014, Gao et al. 2016, Phiri et al. 2018). Due to the lack of Rational Polynomial Coefficient (RPC) sensor model parameters in LA3 metadata, for now, the geometric correction was performed using image-to-image correction (Jensen 2005).

A corresponding Landsat-8 OLI Tier 1 data were used as the reference image. Fifty ground control points (GCPs) were selected, and the root mean square error (RMSE) was kept at less than 1 LA3 pixel size. Before the topographic correction was performed, it was necessary to clip both the DEM and LA3 to the same extent. Therefore, the AOI described in Figure 1 was used as the clipping boundary. Slope and aspect were then derived from the DEM, as shown in Figures 2B and 2C, respectively. Figures 2D, 2E, and 2F show the distribution of terrain elevation, slope and aspect in the study area. In this preliminary study, the topographic correction was performed on LA3

digital number without prior radiometric or atmospheric correction. Each resampling procedure used the nearest neighbour algorithm, due to its ability to preserve the original pixel value (Parker et al. 1983, Zylshal et al. 2017). As explained on previous section, the LA3 DN value was used in further analysis.

Topographic Correction

This initial study focuses on topographic correction using illumination modelling (Pimple et al. 2017). This approach can be categorized into two groups: that which assumes Lambertian conditions, in which the reflectance is independent of the observation angle; and that which considers bidirectional reflectance (non-Lambertian) (Hantson and Chuvieco 2011).

Figure 3 illustrates the illumination modelling (IL) used for the topographic correction. The first step is to calculate the illumination modelling (Riaño et al. 2003) using equation 1 below:

$$IL = \cos \gamma_i = \cos \theta_s \cos \theta_n + \sin \theta_s \sin \theta_n \cos\{\phi_n - \phi_s\} \quad (1)$$

where:
IL – the local solar illumination angle,
θ_n – the solar zenith angle,
θ_s – the terrain slope,
ϕ_n – the solar azimuth,
ϕ_s – the topographic azimuth.
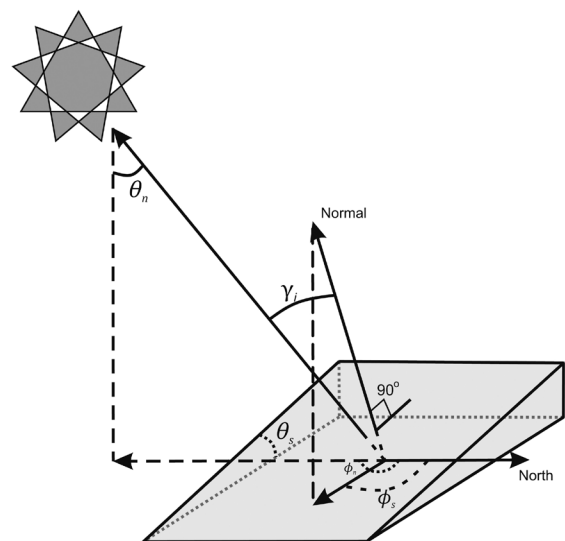
Fig. 3. Geometric illustration shows all angles involved in calculating the incidence angle between normal to the ground and sunrays in slopped area. Image reproduced from Riaño et al. (2003).

DEM was used to obtain θs and ϕ_s. The simplest method is cosine correction, as proposed by Teillet et al. (1982). This algorithm assumes the ground as a Lambertian surface. It is easier to apply since it does not need any external parameters, and is defined as:

$$\rho_H = \rho_T \left(\frac{\cos \theta_n}{IL} \right) \tag{2}$$

where:
ρ_H – the reflectance of a horizontal surface,
ρ_T – the reflectance of a sloped surfaced

While this method is simpler to apply, several studies have found that for the low illuminated areas where $\cos \gamma_i$ is close to zero, it tends to produced overcorrection (Riaño et al. 2003, Gao and Zhang 2009b). Civco (1989) therefore proposed an alternative version of cosine correction by adding average illumination conditions (equation 3). $\overline{IL}$ Denotes the average IL value. Both of these algorithms are independent of the wavelength. One of the most cited non-Lambertian methods was proposed by Minnaert (1941), which was originally used to assess the roughness of the moon's surface, but then more widely adopted in EO data (equation 4).

$$\rho_H = \rho_T + \left[\rho_T \left(\frac{\overline{IL} - IL}{\overline{IL}} \right) \right] \tag{3}$$

$$\rho_H = \rho_T \left(\frac{\cos \theta_n}{IL} \right)^K \tag{4}$$

This approach introduced a *k* factor, which is commonly referred to as the Minnaert constant, whose value ranges from 0 to 1. A *k* value of 1 indicates a perfect Lambertian surface. The k factor is calculated for each band by linearization of equation (4), so equation (4) becomes equation (5) (Riaño et al. 2003)

$$\ln(\rho_T) = \ln(\rho_H) + K \ln \left(\frac{IL}{\cos \theta_n} \right) \tag{5}$$

K and $\ln(\rho_H)$ are the linear regression coefficients, and ρ_H is constant for the whole image (Riaño et al. 2003). Several studies has shown that the Minnaert algorithm has been able to improve accuracy compared to cosine correction (Justice et al. 1981, Itten and Meyer 1993, Richter et al.

2009). Other studies then modified equation (4) to include slope information (Colby 1991, Riaño et al. 2003), as defined below:

$$\rho_H = \rho_T \cos \theta_s \left(\frac{\cos \theta_n}{IL \cos \theta_s} \right)^K \tag{6}$$

Civco (1989) proposed a two stage normalization method. First, a hillshade model is simulated to match illumination conditions based on the Sun's azimuth and elevation at the satellite acquisition time. Each of the original bands is then transformed into a topographically normalized image using equation (7) below:

$$\rho_H = \rho_T + \left(\left(\rho_T \frac{\overline{IL} - IL}{\overline{IL}} \right) C_\lambda \right) \tag{7}$$

where $\overline{IL}$ is the mean value for the south-facing and north-facing slopes, and C_λ is the correction coefficient for each band λ, calculated as equation (8):

$$C_\lambda = \frac{(S_\lambda - N_\lambda)}{\left[\left(N_\lambda \times \frac{\mu_N - \mu_k}{\mu_k} \right) - \left(S_\lambda \times \frac{\mu_S - \mu_k}{\mu_k} \right) \right]} \tag{8}$$

where:
N_λ – the mean of the away-facing slope from the sun for the uncorrected image,
S_λ – the mean of the sun-facing slope,
μ_k – the mean pixel value for all the modelled shaded relief,
μ_N – the mean pixel value for the away-facing slope from the sun,
μ_S – the mean pixel value for the sun-facing slope.

Performance Evaluation

The performance of each algorithm was evaluated using two different assessments, namely qualitative inspection, based on visual appearance, and quantitative evaluation. By comparing the same image before and after correction, visual assessment was used to observe whether there was over/under correction. Overcorrection would result in brighter pixels for the sun-shaded compared to the sun-facing slopes (Gao and Zhang 2009b). Under correction, on the other hand, would result in darker sun-shaded slopes compared to the sun-facing ones.

Under- or overcorrection was also evaluated based on the regression fitting line between the local solar illumination angle (cos γ_i) and the pixel value, before and after correction (Vincini and Frazzi 2003, Gao et al. 2013, Zhang and Gao 2011). A successful correction method should be able to reduce the correlation (r) between cos γ_i and the pixel value. For this purpose, 3942 samples were randomly generated. The pixel value before and after correction, as well as cos γ_i for each sample per band, were then taken and fitted into a linear regression. A t-test was then performed to test the significance at 95% confidence level.

For quantitative analysis, changes in the coefficient variation (CV) of the pixel values before and after correction were used. This method has been widely employed to validate topographic correction (Gao and Zhang 2009b, Hantson and Chuvieco 2011). Changes in CV are also referred to as dispersion indices (Gao and Zhang 2009a, Zhang and Gao 2011).

The sample points previously created were then used to calculate the mean and standard deviation value from both before and after image correction. The coefficient variation was then calculated using equation (9) below:

$$CV(\%) = \frac{\delta}{\mu} \times 100 \qquad (9)$$

where δ is the standard deviation, and μ is the mean pixel values from the samples.

The changes in the CV were then calculated using equation (10) (Richards 1995, Vanonckelen et al. 2014, Pimple et al. 2017, Zylshal 2019):

$$CV_{difference} = CV_{before} - CV_{after} \qquad (10)$$

The $CV_{difference}$ was calculated for each band and each algorithm and the results compared. Successful topographic correction should be able to reduce the variability within each band; that is, giving a positive value of $CV_{difference}$.

Results

Visual comparisons

Figure 4 shows the images resulting from each of the five topographic correction algorithms applied to the AOI. The original image is shown in Figure 4A using a red-NIR-blue composite to better enhance the areas of dense vegetation in the sloped region. Visually, cosine correction (Fig. 4B) performs worst, with visible overcorrection in the hilly region. Improved cosine correction (Fig. 4C) and two-stage normalization (Fig. 4F) are both able to reduce such overcorrection. However, they exhibit an inverse effect, with some of the valleys appearing as hills. Minnaert correction (Fig. 4D), as well as the modified Minnaert (Fig. 4E) performed the best. Both these methods were able to flatten the hilly region and reduce the topographic effect.

Figure 5 shows scatter plots and regression lines between the pixel value and local illumination (cos γ_i) over the near-infrared band for the 3,942 samples taken. Figure 5A shows a clear and statistically significant correlation between the pixel value of the NIR band and local illumination ($R^2 = 0.2837$). Figure 5B confirms the overcorrection shown in Figure 4B, with an increase in the correlation, as well as the regression line being tilted in another direction. Increased correlation is also found in both Figure 5C and 5D (improved cosine correction and two-stage normalization respectively, albeit at not such high levels as with cosine correction. Only the Minnaert correction (Fig. 5D) and modified Minnaert (Fig. 5E) were able to reduce the correlation coefficient, with the latter performing the best, with the highest correlation coefficient reduction (Table 1). Additional quantitative assessment by calculating the coefficient variation before and after correction is shown in Table 1.

For the red and green bands, Minnaert correction performed the best, with the highest correlation coefficient reduction (2.52 and 0.53 respectively). For the blue band, all five correction methods were unable to reduce the correlation coefficient. Minnaert correction performed the best, with the lowest increase in $CV_{difference}$ (−0.16). Observing the number of bands successfully corrected, Minnaert correction and modified Minnaert correction were able to correct three out of the four LA3 bands. The improved cosine correction and the two-stage normalization methods were only able to correct one of the four LA3 bands, while cosine correction performed the worst, with no bands successfully corrected.
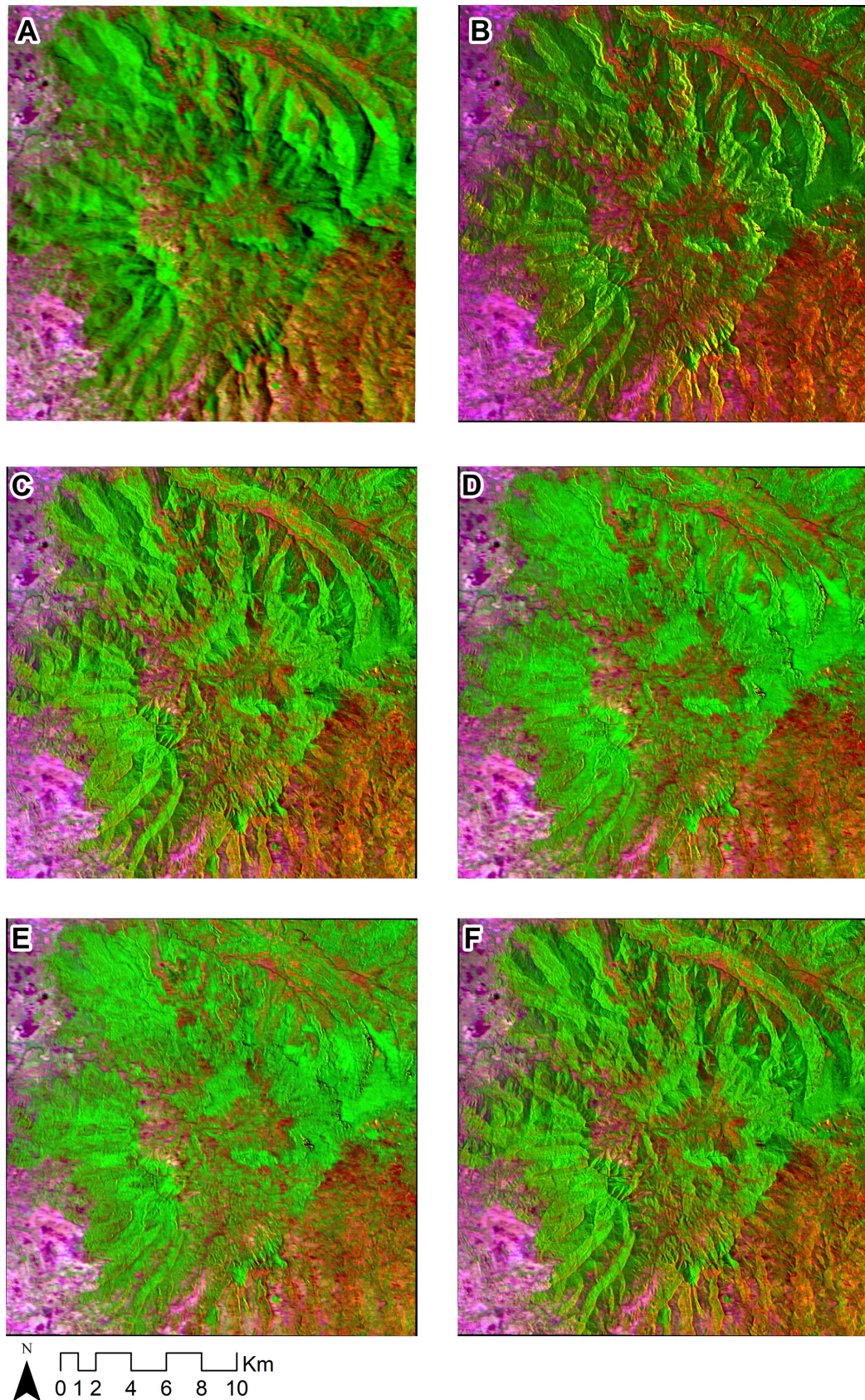
Fig. 4. A – NIR-R-B False color composite of LAPAN-A3 and after applying topographic correction algorithms: B – cosine correction, C –improved cosine correction, D – Minnaert correction, E – modifed Minnaert correction, and F – two-stage normalization.
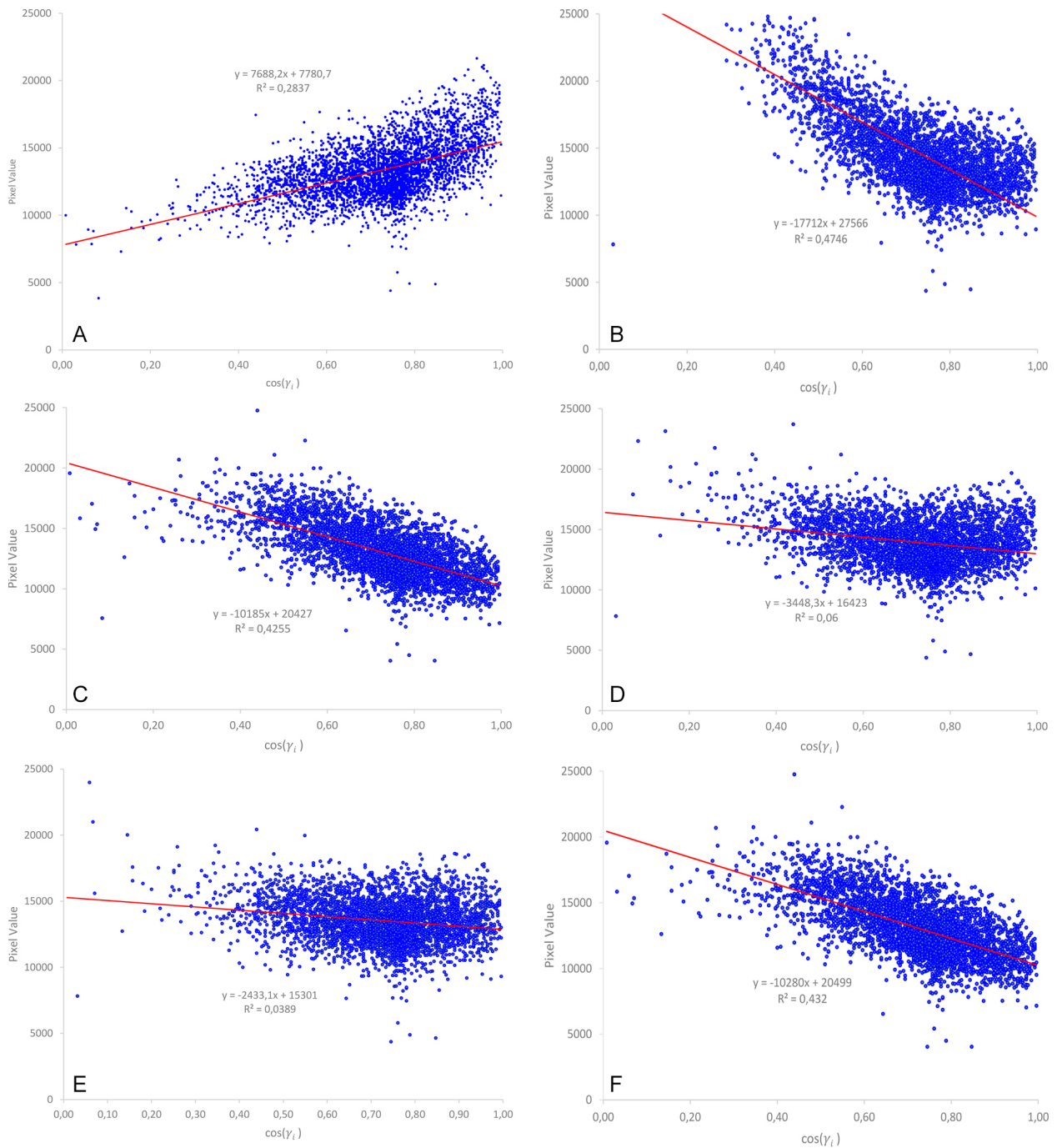
Fig. 5. Scatter plots and regression lines between the pixel value and local illumination (cos γ_i) over Near-infrared band for 3942 taken from both Precorrected (A) and corrected image using: B – cosine correction (Teillet et al. 1982), C – modified-cosine correction (Civco 1989), D – Minnaert correction (Minnaert 1941), E – modified Minnaert correction (Riaño et al. 2003), and F – two-stages normalization (Civco 1989) modified by (Law & Nichol 2004).

Discussion

A strong and statistically significant relationship between local illumination and pixel value has been reported in the literature (Kobayashi and Sanga-Ngoie 2008, Soenen et al. 2008, Wu et al. 2008, Mishra et al. 2009, Zhang and Gao 2011, Vázquez-Jiménez et al. 2017) and is confirmed in this study. The initial objective of this research was to identify which topographic algorithm

performed the best with LA3 data. Previous studies have shown that each algorithm performed differently with different EO satellite data or landform characteristics (Gao and Zhang 2009b, Mishra et al. 2009, Vanonckelen et al. 2014). In this study, the performance of each topographic correction varied for different bands. Cosine correction consistently overcorrected all the LA3 bands. This result is in line with the findings of previous studies (Riaño et al. 2003, Gao et al. 2013, Vanonckelen et al. 2014, Pimple et al. 2017), and is due to Lambertian surface assumptions. The improved cosine correction and two-stage normalization methods performed in a similar fashion to each other. Both of these algorithms only managed to correct the red band, while the other bands showed overcorrection. The negative $CV_{difference}$ value indicates the overcorrection, albeit not as high as with the cosine correction. Only

the Minnaert correction and modified Minnaert correction were consistently able to reduce the correlation coefficient as well as the coefficient of variation (Table 1).

The findings from this study show that Minnaert correction performs best with LAPAN-A3/LAPAN-IPB data. Combined with the initial results from Zylshal (2019), we can confirm that out of the five topographic algorithms tested, the combination of Minnaert correction and ALOS World 3D 30 meter data performed best in correcting the topographic effects of the mountainous region. These results, however, only relate to one type of landform (as described in the previous section), so it is the author's plan to expand the study, by covering different DEM sources with different datasets acquired in different seasons. Different dominant landuse/land-cover such as forests could be well suited for use

Table 1. Statistics of pixel value before and after topographic correction. A negative value indicates an increase in coefficient variation after correction. Bold and highlighted value indicated the best performed algorithm (σ is the standard deviation, cv is the correlation coefficient, and R is the correlation coefficient).

	Algorithm	Stats	Band			
			NIR	R	G	B
Precorrected	Ori	mean	13340.19	8434.89	9639.64	277.14
		σ	2070.84	3007.36	1579.32	533.12
		cv	15.52	35.65	16.38	192.37
Corrected	cosine correction	mean	14757.97	9210.36	10686.45	280.60
		R	0.69	0.29	0.65	0.15
		σ	3688.53	3444.89	2992.48	540.96
		cv	24.99	37.40	28.00	192.79
		$cv_{difference}$	−9.47	−1.75	−11.62	−0.42
	improved cosine correction	mean	13061.56	8196.82	9467.50	258.26
		R	0.65	0.14	0.60	**0.14**
		σ	2239.93	2773.34	1798.05	500.44
		cv	17.15	33.83	18.99	193.77
		$cv_{difference}$	−1.63	1.82	−2.61	−1.40
	Minnaert correction	mean	13929.20	8749.86	10073.39	278.58
		R	0.24	**0.06**	0.28	0.16
		σ	2019.77	2899.01	1615.29	536.34
		cv	14.50	33.13	16.04	192.53
		$cv_{difference}$	1.02	**2.52**	**0.35**	**−0.16**
	modified Minnaert correction	mean	13542.25	8549.51	9819.09	276.68
		R	**0.20**	0.08	**0.21**	0.16
		σ	1764.99	2921.02	1603.82	534.63
		cv	13.03	34.17	16.33	193.23
		$cv_{difference}$	**2.49**	1.49	0.05	−0.86
	two-stages normalization	mean	13061.56	8196.82	9467.50	258.26
		R	0.66	0.14	0.60	**0.14**
		σ	2239.93	2773.34	1798.05	500.44
		cv	17.15	33.83	18.99	193.77
		$cv_{difference}$	−1.63	1.82	−2.61	−1.40

as another method, such as Sun-Canopy-Sensor (SCS) correction (Gu and Gillespie 1998).

The lack of prior atmospheric correction should also be kept in mind with regard to this study findings. By using DN as the pixel value instead of the atmospherically-corrected surface reflectance value, the image data are influenced by diffuse as well as direct irradiance (Richards 1995, Kobayashi and Sanga-Ngoie 2008). Performing prior atmospheric correction would make the topographic correction results more specific by isolating the cause of the differences between pre-correction and post-correction pixel values to the difference in topographic conditions. Several studies have found that coupling atmospheric correction with topographic correction could increase classification accuracy (Kawata et al. 1988, Gao and Zhang 2009a, Zhang and Gao 2011, Vanonckelen et al. 2013, 2014, Fan et al. 2018, Phiri et al. 2018). This study, however, did not employ classification as one of the evaluation methods. Classification accuracy is determined by many factors, not just topographic conditions (Fan et al. 2018), so we decided to focus on an evaluation method that directly shows the influence of the employed topographic correction.

The fact that the study used a freely available DEM makes the potential for reproducibility of the results in similar conditions high. Further improvement and tweaks to the algorithm parameters are also possible, such as performing the topographic correction on TOA reflectance or surface reflectance images, provided that the necessary parameters or products are available for LAPAN-A3 data.

Conclusions

Five different topographic correction algorithms were evaluated on LAPAN-A3 LISA data. Minnaert correction performed the best in terms of visual appearance, correlation coefficient reduction between local illumination and pixel value, as well as the reduction in coefficient variation. Each band reacted differently to all of the algorithms. Minnaert correction as well as modified Minnaert correction were able to successfully correct the topographic effect in the near-infrared, red and green bands. The blue band, however, showed little or no improvement using all five different algorithms.

How well the algorithms perform on LAPAN-A3 with different landforms should be a focus of further research.

References

Balthazar V., Vanacker V., Lambin E. F., 2012. Evaluation and parameterization of ATCOR3 topographic correction method for forest cover mapping in mountain areas [online]. International Journal of Applied Earth Observation and Geoinformation. Elsevier B.V. DOI 10.1016/j.jag.2012.03.010.

Civco D. L., 1989. Topographic Normalization of Landsat Thematic Mapper Digital Imagery. Photogrammetric Engineering and Remote Sensing 55(9): 1303–1309.

Colby J. D., 1991. Topographic normalization in rugged terrain. Photogrammetric Engineering & Remote Sensing 57(5): 531–537.

Fan W., Li J., Liu Q., Zhang Q., Yin G., Li A., Zeng Y., Xu B., Xu X., Zhou G., Du H., 2018. Topographic correction of forest image data based on the canopy reflectance model for sloping terrains in multiple forward mode. Remote Sensing 10(5) 717.

Gao M., Gong H., Zhao W., Chen B., Chen Z., Shi M., 2016. An improved topographic correction model based on Minnaert. GIScience and Remote Sensing 53(2): 247–264.

Gao M., Zhao W., Gong Z., Gong H., Chen Z., Tang X., 2013. Topographic Correction of Zy-3 Satellite Image and Its Effects on Estimation of Shrubs Leaf Biomass in Mountainous Area. International Symposium on Satellite Mapping Technology and Application (ISSMTA2013), WG I/5, WG I/4: 50–59.

Gao Y., Zhang W., 2009a. LULC classification and topographic correction of Landsat-7 ETM+ Imagery in the Yangjia river Watershed: The influence of DEM resolution. Sensors 9(3): 1980–1995.

Gao Y., Zhang W., 2009b. A simple empirical topographic correction method for ETM + imagery. International Journal of Remote Sensing 30(9): 2259–2275.

Ghasemi N., Mohammadzadeh A., Sahebi M. R., 2011. Assessment of different topographic correction methods in ALOS AVNIR-2 data over a forest area. International Journal of Digital Earth 6(5): 504–520. DOI 10.1080/17538947.2011.625049.

Gu D., Gillespie A., 1998. Topographic normalization of Landsat TM images of forest based on subpixel Sun-canopy-sensor geometry. Remote Sensing of Environment 64(2): 166–175.

Hakim P. R., Hasbi W., Syafrudin A. H., 2014. ADCS requirements of Lapan-A3 satellite based on image geometry analysis. Proceeding - ICARES 2014: 2014 IEEE International Conference on Aerospace Electronics and Remote Sensing Technology: 142–146.

Hakim P. R., Permala R., 2017. Analysis of LAPAN-IPB image lossless compression using differential pulse code modulation and huffman coding. In: IOP Conference Series: Earth and Environmental Science. IOP Publishing, 012096. Online: stacks.iop.org/1755-1315/54/i=1/a=012096?key=crossref.1a61d1a04f592578ef866b-15f20559b9 (Accessed 6 March 2017).

Hakim P. R., Syafrudin A. H., Utama S., 2017. Band Co-registration Distortion Modeling of LAPAN-A3 Multispectral Imager Based on Satellite Attitude. The 4th International Symposium on LISAT 2017.

Hantson S., Chuvieco E., 2011. Evaluation of different topographic correction methods for landsat imagery. International Journal of Applied Earth Observation and Geoinformation 13(5): 691–700. DOI 10.1016/j.jag.2011.05.001.

Hasbi W., Suhermanto 2013. Development of LAPAN-A3 / IPB Satellite an Experimental Remote Sensing Microsatellite. In: 34th Asian Conference on Remote Sensing 2013. Online: a-a-r-s.org/acrs/index.php/acrs/acrs-overview/proceedings-1?view=publication&task=show&id=1365.

Holben B. N., Justice C.O., 1980. The Topographic Effect on Spectral Response from Nadir-Pointing Sensors. Photogrammetric Engineering & Remote Sensing 46: 1191–1200.

Itten K. I., Meyer P., 1993. Geometric and Radiometric Correction of TM Data of Mountainous Forested Areas. IEEE Transactions on Geoscience and Remote Sensing 31(4): 764–770.

Japan Aerosapce Exploration Agency, E. O. R. C., 1997. ALOS Global Digital Surface Model 'ALOS World 3D – 30m (AW3D30)' – Product Description. Japan Aerospace Exploration Agency. Online: www.eorc.jaxa.jp/ALOS/en/aw3d30/.

JAXA, 2017. ALOS Global Digital Surface Model (DSM) "ALOS World 3D-30m" (AW3D30) Dataset Product Format Description Earth Observation Research Center (EORC), Japan Aerospace Exploration Agency (JAXA).

Jensen J. R., 2005. Introductory Digital Image Processing: A Remote Sensing Perspective. 3rd Ed. Pearson Education.

Judianto C. T., Nasser E. N., 2015. The Analysis of LAPAN-A3/IPB Satellite Image Data Simulation Using High Data Rate Modem. Procedia Environmental Sciences 24: 285–296. DOI 10.1016/j.proenv.2015.03.037.

Justice C. O., Wharton S. W., Holben B. N., 1981. Application of digital terrain data to quantify and reduce the topographic effect on landsat data. International Journal of Remote Sensing 2(3): 213–230.

Kawata Y., Ueno S., Kusaka T., 1988. Radiometric correction for atmospheric and topographic effects on landsat mss images. International Journal of Remote Sensing 9(4): 1–2.

Kobayashi S., Sanga-Ngoie K., 2008. The integrated radiometric correction of optical remote sensing imageries. International Journal of Remote Sensing 29 (20): 5957–5985.

Law K. H., Nichol J., 2004. Topographic correction for differential illumination effects on ikonos satellite imagery. XXth ISPRS Congress, XXXV Part: 641–646.

Li M., Im J., Beier C., 2013. Machine learning approaches for forest classification and change analysis using multi-temporal Landsat TM images over Huntington Wildlife Forest. GIScience and Remote Sensing 50(4): 361–384.

Minnaert M., 1941. The reciprocity principle in lunar photometry. The Astrophysical Journal 93(2): 403–410.

Mishra V. D., Sharma J. K., Singh K. K., Thakur N. K., Kumar M., 2009. Assessment of different topographic corrections in AWiFS satellite imagery of Himalaya terrain. Journal of Earth System Science 118(1): 11–26.

Nichol J., Hang L. K., 2013. The Influence of DEM Accuracy on Topographic Correction of Ikonos Satellite Images. Photogrammetric Engineering & Remote Sensing 74(1): 47–53.

Nugroho J. T., Zylshal Z., Kushardono D., 2018. LAPAN-A3 Satellite Data Analysis for Land Cover Classificationb (Case Study: Toba Lake Area, North Sumatra). International Journal of Remote Sensing and Earth Sciences 15(1): 71–80.

Parker J. A, Kenyon R. V. and Troxel D. E., 1983. Comparison of interpolation methods for image resampling. IEEE Transactions on Medical Imaging 2(1): 31–39.

Phiri D., Morgenroth J., Xu C., Hermosilla T., 2018. Effects of pre-processing methods on Landsat OLI-8 land cover classification using OBIA and random forests classifier. International Journal of Applied Earth Observation and Geoinformation 73: 170–178.

Pimple U., Sitthi A., Simonetti D., Pungkul S., Leadprathom K., Chidthaisong A., 2017. Topographic correction of Landsat TM-5 and Landsat OLI-8 imagery to improve the performance of forest classification in the mountainous terrain of Northeast Thailand. Sustainability 9(2): 1–26.

Riaño D., Chuvieco E., Salas J., Aguado I., 2003. Assessment of different topographic corrections in landsat-TM data for mapping vegetation types (2003). IEEE Transactions on Geoscience and Remote Sensing 41 (5 PART 1): 1056–1061.

Richards J. A., 1995. Remote Sensing Digital Image Analysis. Berlin/Heidelberg: Springer-Verlag. Online: link.springer.com/10.1007/978-3-642-30062-2 (Accessed 19 September 2017).

Richter R., 1997. Correction of atmospheric and topographic effects for high spatial resolution satellite imagery. International Journal of Remote Sensing 18(5): 1099–1111.

Richter R., Kellenberger T., Kaufmann H., 2009. Comparison of topographic correction methods. Remote Sensing 1(3): 184–196.

Roza W., Amin D. E., Nasser E. N., 2014. Design And Implementation of Payload Data Handling Based on Field Programmable Gate Array. In: 2014 IEEE International Conference on Aerospace Electronics and Remote Sensing Technology (ICARES) Design. Yogyakarta, Indonesia: IEEE: 48–54.

Setiawan Y., Prasetyo L. B., Pawitan H., Liyantono L., Syartinilia S., Wijayanto A. K., Permatasari P. A., Syafrudin A. H., Hakim P. R., 2018. Pemanfaatan Fusi Data Satelit Lapan-a3/Ipb Dan Landsat 8 Untuk Monitoring Lahan Sawah. Jurnal Pengelolaan Sumberdaya Alam dan Lingkungan 8(1): 67–76.

Shao Y., Li G. L., Guenther E., Campbell J. B., 2015. Evaluation of Topographic Correction on Subpixel Impervious Cover Mapping with CBERS-2B Data. IEEE Geoscience and Remote Sensing Letters 12(8): 1675–1679.

Soenen S. A., Peddle D. R., Coburn C. A., Hall R. J., Hall F. G., 2008. Improved topographic correction of forest image data using a 3-D canopy reflectance model in multiple

forward mode. International Journal of Remote Sensing 29(4): 1007–1027.

Tahir A. M., Hakim P. R., Syafruddin A. H., Cagak J., Km S., Indonesia B., 2016. Image-Focusing Quality Improvement on Lapan-A3 Satellite Multispectral Imager. Jurnal Teknologi Dirgantara 14(1): 37–50.

Takaku J., Tadono T., 2017. Quality updates of 'AW3D' global DSM generated from ALOS PRISM. 2017 IEEE International Geoscience and Remote Sensing Symposium (IGARSS): 5666–5669.

Takaku J., Tadono T., Tsutsui K., Ichikawa M., 2016. Validation of 'Aw3D' Global Dsm Generated From Alos Prism. ISPRS Annals of Photogrammetry, Remote Sensing and Spatial Information Sciences III–4 (July): 25–31.

Teillet P. M., Guindon B., Goodenough D. G., 1982. On the slope-aspect correction of multispectral scanner data. Canadian Journal of Remote Sensing 8(2): 84–106.

Triharjanto R. H., Nur Ubay M. S., Utama S., Poetro R. E., 2016. Evaluation of attitude dynamic module on LAPAN-ITB micro-satellite simulator. In: Proceedings of the 2015 IEEE International Conference on Aerospace Electronics and Remote Sensing, ICARES 2015. Bali, Indonesia: IEEE.

Vanonckelen S., Lhermitte S., Balthazar V., Van Rompaey A., 2014. Performance of atmospheric and topographic correction methods on Landsat imagery in mountain areas. International Journal of Remote Sensing 35(13): 4952–4972.

Vanonckelen S., Lhermitte S., Van Rompaey A., 2013. The effect of atmospheric and topographic correction methods on land cover classification accuracy. International Journal of Applied Earth Observation and Geoinformation 24(1): 9–21. DOI 10.1016/j.jag.2013.02.003.

Vázquez-Jiménez R., Romero-Calcerrada R., Ramos-Bernal R., Arrogante-Funes P., Novillo C., 2017. Topographic Correction to Landsat Imagery through Slope Classification by Applying the SCS + C Method in Mountainous Forest Areas. ISPRS International Journal of Geo-Information 6(9): 287.

Vincini M., Frazzi E., 2003. Multitemporal Evaluation of Topographic Normalization Methods on Decidous Forest TM Data. IEEE Transactions on Geoscience and Remote Sensing 41(11): 2586–2590.

Wu J., Bauer M. E., Wang D., Manson S. M., 2008. A comparison of illumination geometry-based methods for topographic correction of QuickBird images of an undulant area. ISPRS Journal of Photogrammetry and Remote Sensing 63(2): 223–236.

Zhang W., Gao Y., 2011. Topographic correction algorithm for remotely sensed data accounting for indirect irradiance. International Journal of Remote Sensing 32(7): 1807–1824.

Zylshal Z., 2019. Performance evaluation of different DEMs for topographic correction on LAPAN-A3: preliminary results. In: Sixth Geoinformation Science Symposium SPIE: 159–167.

Zylshal Z., Sari N. M. N. M., Nugroho J. T. J. T., Kushardono D., 2017. Comparison of Spectral Characteristic between LAPAN-A3 and Sentinel-2A. IOP Conference Series: Earth and Environmental Science 98(1): 012051.

Zylshal Z., Wirawan R. R., Kushardono D., 2018. Assessing the Potential of LAPAN-A3 Data for Landuse/landcover Mapping. Indonesian Journal of Geography 50(2): 184–196. DOI 10.22146/ijg.31449.